

Data-driven detrending of nonstationary fractal time series with echo state networks

Enrico Maiorino^{*1}, Filippo Maria Bianchi^{†1}, Lorenzo Livi^{‡§2}, Antonello Rizzi^{¶1}, and Alireza Sadeghian^{||2}

¹Dept. of Information Engineering, Electronics, and Telecommunications, SAPIENZA University of Rome, Via Eudossiana 18, 00184 Rome, Italy

²Dept. of Computer Science, Ryerson University, 350 Victoria Street, Toronto, ON M5B 2K3, Canada

April 30, 2022

Abstract

In this paper, we propose a data-driven approach to the problem of detrending fractal and multifractal time series. We consider a time series as the measurements elaborated from a dynamical process over time. We assume that such a dynamical process is predictable to a certain degree, by means of a class of recurrent networks called echo state networks. Such networks have been shown to be able to predict the outcome of a number of dynamical processes. Here we propose to perform a data-driven detrending of nonstationary, fractal and multifractal time series by using an echo state network operating as a filter. Notably, we predict the trend component of a given input time series, which is superimposed to the (multi)fractal component of interest. Such a (estimated) trend is then removed from the original time series and the residual signal is analyzed with the Multifractal Detrended Fluctuation Analysis for a quantitative verification of the correctness of the proposed detrending procedure. In order to demonstrate the effectiveness of the proposed technique, we consider several synthetic time series having a self-similar noise component with known characteristics. Such synthetic time series contain different types of trends. We also process a real-world dataset, the sunspot time series, which is well-known for its multifractal features and it has recently gained attention in the complex systems field. Results demonstrate the validity and generality of the proposed detrending method based on echo state networks.

Keywords— Fractal and multifractal time series; Fluctuation analysis; Detrending; Echo state network; Prediction.

1 Introduction

Memory is one of the most interesting aspects of many processes in Nature and society [17]. In order to characterize and predict a system with memory, it is necessary to keep into account its past history. Memory can be quantified in different ways depending on the particular features and effects one wants to highlight. One of the most common approaches in the study of real-valued time series is the analysis of the autocorrelation function. In such a linear setting, the extent of memory can be roughly quantified as the characteristic time scales at which the series remains correlated, i.e., through the decay of the autocorrelation function. When the decay is exponential, the series is said to manifest *short-memory* and the influence of the past to the current state is limited in time. When, instead, the decay follows a

*enrico.maiorino@uniroma1.it

†filippomaria.bianchi@uniroma1.it

‡llivi@scs.ryerson.ca

§Corresponding author

¶antonello.rizzi@uniroma1.it

||asadeghi@ryerson.ca

power-law, then there is no characteristic scale in the autocorrelation, i.e., the influences of the past have no cut-off. In this case, a time series is said to manifest *long-term memory* or *long-term correlation* (LTC) and the strength of this correlation is referred to as degree of *persistence* of the generating stochastic process. Persistence of a stochastic process [38] is quantified by the self-similarity coefficient, called Hurst exponent $H \in [0, 1]$. A straightforward numeric way to estimate the Hurst coefficient is the Fluctuation Analysis (FA), which evaluates the slope of the fluctuations scaling function $F(s)$. This function is in turn calculated by dividing the integrated time series in segments of equal sizes s and evaluating the root mean square difference between their extremal points. When the process corresponds to uncorrelated noise (e.g., white Gaussian noise), then the value of H is 0.5, whereas if the process is persistent (correlated) or antipersistent (anticorrelated) it will be respectively greater than or less than 0.5.

However, conventional methods employed to analyze the LTC properties of a time series (e.g., FA, spectral analysis, R/S analysis [2, 40, 41]) are misleading when such time series are non-stationary [7]. In fact, in many cases a process is driven by underlying trends [21], which operate at specific time scales, like seasons in the analysis of data related to a natural phenomenon and days in financial market analysis. Usually, when investigating memory properties of a process, one is interested in the fractal properties of the intrinsic fluctuations of such a process. Several methods have been proposed to extract and analyze the fluctuations of the stationary component of a time series, like detrended fluctuation analysis (DFA), detrended moving average, wavelet leaders [43], adaptive fractal analysis [37], and the so-called geometric-based approaches [15]. Notably, DFA has been shown to be successful in a broad range of applications [24, 27, 41]. The DFA has been generalized in the so-called Multifractal Detrended Fluctuation Analysis (MFDFA) [3, 8, 25, 34], which accounts for multiple scaling exponents. Although DFA and the related variants provide a way to detrend data by means of window-based local (polynomial) fittings, trends are often defined in terms of periodicities and/or fast-varying functions, resulting thus in a spurious detection of fractality [18]. For this reason, additional detrending methods are often used as a preprocessing step of the (MF-)DFA to single out these trends before the polynomial detrending takes place. In other works, the local detrending step of DFA is modified or replaced with other ad-hoc methods [20, 26, 36].

The main problem with detrending lies in the difficulty of defining what exactly a trend is [44]. In local-fit based methods, the underlying assumption is the fact that a trend is generally a slow-varying process on which is superimposed a noise process having higher frequencies. While this is often the case, it is still difficult to determine the right form and parameters of the fitting function without biasing the analysis. Moreover, window-based fitting algorithms are heavily influenced by the choice of the window sizes. In Ref. [44] a trend is defined as an intrinsically determined monotonic function within a certain temporal span, or as a function in which there can be at most one extreme within that temporal span. This method is not affected by border effects since it is not window-based. However, a problem with this definition is that it does not (fully) describe periodic trends in a consistent way. Chianca et al. [9] suggested to perform a detrending by applying a simple low-pass filter, in order to eliminate slow periodic trends from data. While this approach is suitable for systems with slow-varying trends, it is difficult to apply it in more general cases, when the trends' frequencies span over a significant portion of the (power) spectrum. Another approach that has been demonstrated to be useful in the case of periodicities was proposed by Nagarajan [33]. As a first step, the signal is represented as a matrix, whose dimension has to be much larger than the number of frequency components of the periodic (or quasi-periodic) trends as shown by the power spectrum. The well-known singular value decomposition method is then applied in order to remove components related to large-magnitude eigenvalues – corresponding to the trend. Such a method, although interesting and well-founded on the mathematical side, is very demanding in terms of computations and also assumes a deterministic form for trends.

In this work, we follow an approach similar to Wu et al. [44] and define a trend in a completely data-driven way. We consider a time series as the measurements performed on/elaborated from a dynamical process. We assume that the dynamical process is predictable to a certain degree by means of a particular type of Recurrent Neural Network (RNN) called Echo State Network (ESN) [5, 6, 31]. RNNs have been shown to be able to predict the outcome of a number of dynamical processes [11]. However, not all processes are predictable at the same level, as formally studied in [4, 10], for instance. For example, chaotic processes are not predictable for long time-steps, while other deterministic systems, like a sinusoidal waveform, can be easily predicted. When considering a stochastic setting, instead, we note that white Gaussian noise cannot be predicted at all, since the past stores no information about the future. On the other hand, correlated noise signals, such as fractional Gaussian noise (fGn), are in

theory more predictable given the presence of memory in the process. The difficulty of the prediction problem can be reasonably associated also to the complexity of the adopted prediction model and the size of the available training dataset. The more complex the prediction model is, the more it would be capable to predict complex processes given a suitable design and training. In the case of ESNs, the complexity of the model is mainly determined by the properties of the reservoir, e.g., the number of neurons, their connectivity, and the spectral radius. Here we propose to perform a data-driven detrending of nonstationary, fractal and multifractal time series by using ESNs acting as a filter. Notably, by means of an ESN we predict the trend (hence in this study trends are the only form of nonstationarities that we consider) of a given input time series, which is always superimposed to the (multi)fractal component of interest. Such a trend is then removed from the original time series and the residual signal is analyzed with MF DFA in order to evaluate its scaling properties.

The remainder of the paper is structured as follows. In Section 2, we introduce a research field called *neural filtering*, which provides a theoretical support for the proposed detrending method based on ESNs. In Section 3 we present the details of how we perform the detrending with an ensemble of ESNs. Notably, we employ an ensemble of ESNs with fixed complexity (i.e., network sizes and connectivities) to separate (multi)fractal signals from the trends. In Sec. 4 we show and discuss the experimental results obtained on a number of time series, both synthetic and representing real processes. Finally, concluding remarks are discussed in Section 5. This paper contains two appendices: Appendix A introduces the procedure adopted in this study for analyzing LTC and multifractality of time series, while in Appendix B we provide some necessary technical details regarding ESNs.

2 Neural filtering

The main assumption of our model is that the time series under analysis is composed of two superimposed components of different degrees of predictability:

- a trend process $x(t)$, which corresponds to the main underlying stochastic process. This process represents the intrinsic dynamical evolution of the studied system and it is predictable, with high accuracy by an ESN;
- a noise process $n(t)$, which is generally of lower magnitude and it is less predictable by an ESN, i.e., requires higher model complexities.

Notably, we consider a time series $y(t)$ as a mixture composed by a trending signal $x(t)$ with a superimposed zero-mean noise, $n(t)$,

$$y(t) = x(t) + n(t), \quad t \in \mathbb{N}. \quad (1)$$

The trend, $x(t)$, is a nonstationary stochastic process of larger magnitude with respect to $n(t)$, even if there are no hard constraints on their relative scales. The noise process is a self-similar, stationary stochastic process characterized by a Hurst coefficient and, in general, a multifractal spectrum. Prototypical examples of such a process are fractional Gaussian noise and (fractional) Lévy stable processes [17, 38].

The goal of this work is to separate $y(t)$ in its components $x(t)$ and $n(t)$, in order to identify and eventually retain the stationary component, $n(t)$. To achieve this, we approach the problem as a prediction task in the formal framework of neural filtering [28–30]. A discrete-time optimal filter is a dynamical system that takes in input $y(t)$ and outputs an estimate, $\hat{x}(t)$, of $x(t)$ at each time step t , such that a given error criterion (e.g., mean square error) is optimized. The dynamical state of the optimal filter at time t must contain the optimal conditional statistics given all the measurements $y(t)$ observed up to time t . Neural filtering is a framework in which Artificial Neural Networks (ANN) are used for estimating signals generated by stochastic processes whose characteristics change unexpectedly or suddenly as a result of disturbances, faults, etc. The network is synthesized with the observed data of the underlying process and it does not require assumptions on the dynamics of the process or the nature of the noise. A fundamental theorem [28] states that an RNN exists that takes as input the measurement process and outputs an estimate of the signal process, where the estimate can be made as close as desired to the conditional expectation of the signal process given the past history of the measurement process that has been processed. Hence, a properly trained neural filter with a proper architecture approximates

the optimal filtering performance to any accuracy level. In addition, the filtered signal carries the most informative statistics in its dynamical state.

Many ANN models have been used, but not all achieved satisfying performances. At present, Recurrent MultiLayer Perceptrons (RMLPs) are believed to be the best approach [30]. An RMLP is a feed-forward ANN whose processing nodes compute the weighted average of its inputs and then apply an activation function such as the hyperbolic tangent. After a unit-time delay, the activation levels of the processing nodes is used as feedback to processing nodes in the same or a lower layer [35].

In our study, we propose to use ESNs as filters in order to estimate the trend, $x(t)$, in the observed signal $y(t)$. Technical details about the ESN model are reported in Appendix B. ESNs benefit from feedbacks like other RNNs, which allow to model any complex dynamic behavior. In addition, ESNs use a sparsely interconnected reservoir of neurons that leads to a very fast and simple training procedure – unlike the complicated and time consuming training process required by classic RNNs.

3 Detrending using ESNs

As mentioned above, we approach the problem of detrending a time series $y_{\text{data}}(t)$ as an ESN-based prediction problem. The first step consists in splitting $y_{\text{data}}(t)$ in two separate datasets: the training $y_{\text{tr}}(t)$ and the test $y_{\text{ts}}(t)$ datasets. In fact, to avoid overfitting we train the ESN readout on the training data and predict the values of the test data. The predicted test data is in turn utilized to detrend $y_{\text{ts}}(t)$ as explained below. The separation between training and test data implies that only the test data is effectively detrended. From now on, for ease of notation, we will denote $y_{\text{ts}}(t)$ simply as $y(t)$ and assume that the training step has already been performed.

Let $y(t) = x(t) + n(t)$ be a time series which describes the observable value of an underlying dynamical system, whose signal is represented by $x(t)$ and $n(t)$ is the noise. We denote with $\hat{y}(t)$ the time series composed by the predicted values of $y(t)$ by using an ESN. It can be expressed as:

$$\hat{y}(t) = y(t) + e_{\text{pred}}(t) = x(t) + n(t) + e_{\text{pred}}(t), \quad t \in \mathbb{N}, \quad (2)$$

where $e_{\text{pred}}(t)$ is by definition the ESN prediction error as a function of time.

The performance of a prediction model can be evaluated through the forecast accuracy, typically implemented as the root mean square error (RMSE) [12], quantifying the differences between predicted and observed values. For a given model complexity, the prediction error is related to the amount of training data and on the accuracy of the training procedure. However, even for a optimally trained model, in the presence of noise the forecast will always be subject to an error, due to (intrinsic) stochastic unpredictability of the process or insufficient complexity of the prediction model. We refer to this source of error as *intrinsic unpredictability* of the process with respect to the given model complexity and its related error function as $e_{\text{intr}}(t)$. By assuming independence between the training error $e_{\text{tr}}(t)$ and the intrinsic error $e_{\text{intr}}(t)$, we can write $e_{\text{pred}}(t)$ as the sum of the independent components

$$e_{\text{pred}}(t) = e_{\text{tr}}(t) + e_{\text{intr}}(t), \quad t \in \mathbb{N}. \quad (3)$$

If the prediction model is properly trained, we can assume the training error to be negligible, i.e.,

$$e_{\text{tr}}(t) \simeq 0 \quad \forall t \in \mathbb{N}. \quad (4)$$

Our assumption in this work is that the trend process $x(t)$ of the observed signal $y(t)$ is completely predictable by an ESN model and all sources of intrinsic unpredictability are concentrated in the noise component $n(t)$. This assumption corresponds to approximating:

$$\hat{y}(t) \simeq x(t) \quad \forall t \in \mathbb{N}. \quad (5)$$

When Eqs. (4) and (5) hold, by inserting Eq. (3) in (2) we obtain

$$n(t) \simeq -e_{\text{intr}}(t) \quad \forall t \in \mathbb{N}. \quad (6)$$

In this case, the predicted time series, $\hat{y}(t)$, is a good approximation of the trend component $x(t)$ of $y(t)$. Therefore, an estimation $\hat{n}(t)$ of the noise $n(t)$ can be calculated as:

$$\hat{n}(t) \equiv y(t) - \hat{y}(t) = -e_{\text{pred}}(t) \simeq -e_{\text{intr}}(t). \quad (7)$$

The time series that we analyze here contains measurements of a signal with a superimposed noise, which increases the difficulty of obtaining high reliability in short-term forecasts. For this reason, one needs to wait until the trend accumulates sufficiently to break through the noise before it becomes clear: considering different forecast horizons could significantly influence the result of the prediction. In order to mitigate the dependency of the prediction performance on the particular forecast horizon, we perform multiple forecasts using an ensemble of k independent ESNs, each one trained considering a different prediction step m_k . The output signals of the ensemble of predictors, elaborated on the basis of the same input data but using different forecast horizons, generate independent outcomes that are combined together in a resulting forecast, $\hat{y}(t)$. This provides a more accurate prediction by compensating for individual errors or bias introduced by the single predictors.

Such an approach shares some similarity with the well-known framework of ensemble learning [42] and neural network ensembles [19], where in the latter it was showed experimentally that the synergy of multiple back-propagation neural networks improved learning, generalization capability, noise tolerance, and self-organization with respect to a single, yet more complex system.

4 Experimental results

In this section, we evaluate the performance of the proposed detrending method based on ESN – denoted as DESN in what follows – by comparing the results obtained using several well-known detrending methods introduced in Sec. 4.1. These include Empirical Mode Decomposition (EMD), Fourier-Detrend Fluctuation Analysis (FDFA), and different Smoothing (SM) techniques. In order to demonstrate the effectiveness of the proposed technique, we consider several synthetic time series having a self-similar noise component with known characteristics. We also process a real-world and well-known dataset, the sunspot time series – Sec. 4.3. Such data have already been studied in the (multi)fractal analysis context – see [13, 20] and references therein.

4.1 Detrending methods

In this section, we describe some existing methodologies that have been used in previous works for separating trends from the noise components in a time series [3]. To be consistent with our approach, we consider the following detrending procedures as preprocessing steps of the MFDFA.

Empirical Mode Decomposition EMD is a data-driven technique that performs a decomposition of the original signal, $y(t)$, in terms of a finite number of modes, $g_i(t)$, called Intrinsic Mode Functions (IMF). IMFs are derived directly from the data, without any prior assumption about their model. EMD [16] can be used to extrapolate a trend in the data by considering the residual, which is given by: $x(t) = y(t) - \sum_{i=1}^n g_i(t)$. The residue is then subtracted from the original signal in order to remove the global trend. However, Wu et al. [44] showed that, in addition to the residual $x(t)$, also a number of IMFs could be used in order to better approximate the trend. This is especially needed where the trend is composed by periodicities, which cannot be approximated by a single residue. It is worth citing also applications of EMD as a local detrending method used in the windows computed with DFA, in place of the conventional polynomial fitting [36].

Fourier-Detrended Fluctuation Analysis The Fourier-Detrended Fluctuation Analysis (FDFA) is a tool used for analyzing trends having frequencies with significant power [32]. The method targets the first few coefficients (those having larger amplitude or real part) of a Fourier expansion and thus it can be considered as a simple high-pass filter [9]. We use a slightly different approach here, in order to cut the spectral components with higher amplitude, rather than exclusively focusing on those having lower frequencies – as originally proposed in [9]. In this way, the definition of trends is relaxed in order to consider all larger amplitude periodicities, independently of their variation speed. At first, we apply the discrete fast Fourier transform to the data records, then we sort the spectral components according to a decreasing order of their amplitude. Then we truncate the first τ_{freq} coefficients of the Fourier expansion. Finally, we apply the inverse Fourier transform to the truncated series. After this last step, *border effects* may appear at the opposite ends of the time series. These distortions are eliminated by cropping a portion of the initial and last part of the series.

Smoothing Smoothing methods operate in the time domain and basically implement low-pass filters. High frequency are attenuated on the base of the specific properties of the adopted smoothing method. We consider four different smoothing procedures, which depend on a parameter σ , representing the span of the smoothing procedure:

- Algorithm 1: a low-pass filter with coefficients equal to the reciprocal of the span (moving average);
- Algorithm 2: local regression using weighted linear least squares and a 1st degree polynomial model;
- Algorithm 3: local regression using weighted linear least squares and a 2nd degree polynomial model;
- Algorithm 4: a generalized moving average with filter coefficients determined by an unweighted linear least-squares regression and a polynomial model of specified degree p .

4.2 Synthetic time series

In this section, we process a number of synthetically generated time series of the form $y(t) = x(t) + n(t)$, which are composed by a trend component, $x(t)$, and a noise component, $n(t)$. We use the four aforementioned detrending methods for computing an estimation of $y(t)$, namely $\hat{y}(t)$, and we evaluate the accuracy of each method by analyzing the LTC and multifractal properties of the estimated noise, $\hat{n}(t) = y(t) - \hat{y}(t)$. The accuracy of each method is evaluated by comparing the coefficients obtained with MF DFA (see Appendix A) on the estimated noise, $\hat{n}(t)$, with respect to the ground-truth $n(t)$. For all series and methods, the MF DFA procedure has been executed on scales ranging from 16 to 1024 data points and with a second-order local polynomial detrending. The parameter q ranges from -5 to +5.

We consider seven time series Y1, ..., Y7, which are obtained by combining a trend (selected from one of the five different time series X1, ..., X5) with a noise (selected from one of the three different time series n1, n2, and n3). Signals used as trend are described by the functions shown in Table 1. For the trend signals, X1, X2, X4, and X5, we report the interval from which the values of the domain variable x are extracted. In Table 2, are summarized the average properties of the synthetic noise components. We use two different sets of ten fGn processes generated by setting H respectively to 0.7 and 0.3, and a deterministic binomial multifractal cascade [34] with multiplicative factor equal to 0.60708. The spectrum width $\Delta\alpha$ is calculated as the width of the support of the multifractal spectrum $D(\alpha)$, i.e., as $\Delta\alpha = \alpha_{\max} - \alpha_{\min}$. For the noise n3, we also consider the spectrum asymmetry, denoted as Θ , whose value is defined as

$$\Theta = \frac{\Delta\alpha_L - \Delta\alpha_R}{\Delta\alpha_L + \Delta\alpha_R}, \quad (8)$$

where $\Delta\alpha_L$ and $\Delta\alpha_R$ are, respectively, the width of the left and right part of $D(\alpha)$. A negative value of Θ denotes a right-sided spectrum, highlighting a stronger multifractality on smaller fluctuations, while the contrary holds for a positive value.

All time series have been normalized by calculating the z-score; the amplitudes of signal and noise series are multiplied by a suitable scalar value, in order to obtain a signal-to-noise ratio of 16.

Table 1: Description of the functions used as trend within the synthetic signals. The term ν_{\max} refers to the Nyquist frequency $f_s/2$, where f_s is the sampling rate, and the terms $\mathcal{U}(x_{\min}, x_{\max})$ and $\mathcal{N}(\mu, \sigma)$ are respectively the uniform and normal distributions.

ID	Description
X1	$\sin(t)$.
X2	$\sum_{i=1}^{10} A_i \sin(2\pi\nu_i t)$, $\{\nu_i = \mathcal{U}(0, 10^{-5}\nu_{\max})\}$, $\{A_i = \mathcal{N}(1, 1)\}$.
X3	$s\ s\ s\ \dots$, with s the first 100 digits of π .
X4	$\sum_{i=1}^{10} A_i \sin(2\pi\nu_i t)$, $\{\nu_i = \mathcal{U}(0, 0.5\nu_{\max})\}$, $\{A_i = \mathcal{N}(1, 1)\}$.
X5	$\sin(t)/t^2$.

Table 2: Characteristics of the synthetic noise processes. The Hurst exponent and MFW of **n1** and **n2** are the outcome of MFDDFA averaged over ten independent realizations of the process.

ID	Description	Length	avg. Hurst	avg. MFW (Θ)
n1	fGn	150000	0.695	0.022
n2	fGn	150000	0.303	0.032
n3	Binomial cascade	131072	0.883	1.192 (0.048)

Overall, we performed seven different tests. In Table 3, we report the time series under consideration and the values used for configuring each detrending procedure. Note that the length of the i -th time series Y_i is given by the length of the noise component, which is reported in Table 2. Additionally, for the DESN procedure we consider an additional time series for training the network (referred as $y_{tr}(t)$ in Sect. 3), whose length is half of Y_i 's length.

Table 3: Time series and configuration of the different detrending procedures used in each test. For DESN, we report the values of the size of the reservoir (N_r), the spectral radius (ρ), the regularization coefficient (λ), and the number k of forecast models. For FDFA, we report the thresholds τ_{freq} and τ_{time} used for determining the amount of coefficients to be truncated in both frequency and time domain. For SM, we report the span of the moving average σ and the identifier of the adopted algorithm. Finally, for EMD we report the number of the last s IMFs which are used for defining the trend.

Data	DESN	FDFA	SM	EMD
$Y_1 = X_1 + n_1$	$N_r = 500, \rho = 0.99,$ $\lambda = 0.1, k = 30$	$\tau_{freq} = 8, \tau_{time} = 50$	$\sigma = 250, \text{ algo: } 2$	$s = 13$
$Y_2 = X_2 + n_1$	$N_r = 200, \rho = 0.4,$ $\lambda = 0.1, k = 10$	$\tau_{freq} = 60, \tau_{time} = 1$	$\sigma = 1800, \text{ algo: } 3$	$s = 5$
$Y_3 = X_3 + n_1$	$N_r = 500, \rho = 0.99,$ $\lambda = 0.1, k = 20$	$\tau_{freq} = 115, \tau_{time} = 50$	$\sigma = 20, \text{ algo: } 4$	$s = 19$
$Y_4 = X_4 + n_1$	$N_r = 400, \rho = 0.99,$ $\lambda = 0.1, k = 10$	$\tau_{freq} = 1000, \tau_{time} = 3000$	$\sigma = 10, \text{ algo: } 1$	$s = 17$
$Y_5 = X_5 + n_1$	$N_r = 100, \rho = 0.99,$ $\lambda = 0.05, k = 30$	$\tau_{freq} = 4000, \tau_{time} = 250$	$\sigma = 1000, \text{ algo: } 1$	$s = 8$
$Y_6 = X_1 + n_2$	$N_r = 500, \rho = 0.99,$ $\lambda = 0.1, k = 30$	$\tau_{freq} = 400, \tau_{time} = 2000$	$\sigma = 50, \text{ algo: } 2$	$s = 17$
$Y_7 = X_1 + n_3$	$N_r = 500, \rho = 0.99,$ $\lambda = 0.05, k = 20$	$\tau_{freq} = 250, \tau_{time} = 2000$	$\sigma = 60, \text{ algo: } 4$	$s = 24$

Each outcome is the averaged value obtained from performing the test ten times by changing the random seed. The sources of randomness for each test are the different realizations of the noise process – for **n1** and **n2** – and the different executions of the DESN procedure – input and reservoir weights. We used a grid search to tune the (hyper-)parameters of the different methods in their respective spaces. For each detrending method, we considered a different sets of bounds and search resolutions of the respective parameter space and a specific loss function for guiding the optimization. The error measurement that

we used is the Normalized Root Mean Squared Error (NRMSE) function, which is defined as follows:

$$\text{NRMSE}(\hat{y}, y) = \frac{\sqrt{\frac{1}{T} \sum_{t=1}^T (\hat{y}(t) - y(t))^2}}{\max(y) - \min(y)}, \quad (9)$$

being $\hat{y}(t)$ the predicted series and $y(t)$ the measurement process.

For DESN, the parameters that we considered are the size N_r of the reservoir, searched in $[100, 500]$ with resolution 100; the spectral radius ρ searched in $[0.4, 0.99]$ with resolution 0.1; the regularization coefficient λ used in the linear regression for the training of the readout is searched in $[0.05, 0.3]$ with resolution 0.05; the number k of forecast models used is searched in $[10, 30]$ with resolution 10. As discussed in Sec. 3, we used a different forecast step for training each ESN. In particular, relative to the k -th predictor model, we set the forecast step $m_k = 10 \cdot k$. The adopted loss function is the average error computed on the original values y and the forecast \hat{y}_i of the i -th prediction model, that is, $1/k \sum_{i=1}^k \text{NRMSE}(\hat{y}_i, y)$.

For the SM procedure, we tuned the span of the moving average σ in $[10, 2000]$ with resolution 10. For guiding the hyper-parameter optimization, we used a loss function which minimizes the error and maximizes the span, defined as: $f_{\text{SM}} = \eta_{\text{SM}} \cdot \text{Err} + (1 - \eta_{\text{SM}})1/\sigma$, where Err is the error evaluated with Eq. 9 and $\eta_{\text{SM}} \in [0, 1]$ is a weight parameter that was set to 0.1 in every test. Note that for $\eta_{\text{SM}} = 0$ the error component is neglected, then the resulting span is maximized covering the whole time series; this generates a smooth function which contains in every point the mean value of the original signal. On the other hand, by setting $\eta_{\text{SM}} = 1$, only the error is minimized and the span assumes its minimum value $\sigma = 2$, which generally produces an insufficient smoothing of the signal. We evaluated the performances using all the four algorithms described in Sect. 4.1 and we reported here the one which achieved the best results. The polynomial degree p in the algorithm 4 was set to 15 in every test.

For setting the optimal values of the parameter τ_{freq} in the FDFA procedure, after having ordered the Fourier coefficients by their amplitude (from larger to smaller), by visual inspection we first identify the “elbow” in the sequence, which is its inflection point, which determines the frequencies whose amplitudes are largest in the spectrum and that must be truncated. Once the inverse Fourier transform is performed, some cropping on the boundaries of the time series is necessary to attenuate boundary effects caused by the alteration of the spectrum.

Finally, in the EMD approach we used the standard setup of the stop criterion for retrieving the IMFs, as described in [22]. The sum of the last s IMFs represents the trend and the number s is optimized by minimizing the following loss function: $f_{\text{EMD}} = \eta_{\text{EMD}} \text{Err} + (1 - \eta_{\text{EMD}})s/S$, where S represents the total number of IMFs identified relative to each signal – usually they are 15-20. Also in this case, Err is the error evaluated with Eq. 9 and $\eta_{\text{EMD}} \in [0, 1]$ is a weight parameter. Note that for $\eta_{\text{EMD}} = 0$ the error component is neglected and s assumes its minimum value (1), i.e. only the last IMF is selected for approximating the trend. On the other hand, when $\eta_{\text{EMD}} = 1$ the error is minimized, but all the S IMFs are selected for representing the trend, which then coincides with the original signal. We set $\eta_{\text{EMD}} = 0.1$ when we tested the synthetic signals Y3, Y4, Y6, and Y7, while in the processing of the remaining signals (including the sunspot time series) we used $\eta_{\text{EMD}} = 0.5$.

In Fig. 1 we plot a short sample of each time series with superimposed the trends identified by the different detrending procedures. The details of the results are reported in Table 4, where we show the resulting Hurst coefficient and multifractal spectrum width (MFW) for each time series. In Fig. 2 we graphically represent the quality of the fluctuation function scaling for the estimated noise.

As shown in Table 4, the four methods have significant differences in performance on different time series. We could not obtain a correct scaling for most of the tested time series with the EMD and SM methods – considering the parameter optimization criteria presented in Sec. 4.1. The first five time series, Y1-5, are composed by a signal with a superimposed persistent noise with $H = 0.7$.

In the first time series, Y1, the signal is a low-frequency sinusoid. The sinusoid is the simplest periodic function and it is easily separable from the noise, which is much more complex from a prediction perspective. In fact, the Hurst exponent is easily estimated with sufficient precision by DESN. FDFA, as expected, obtains similar results with respect to DESN, since this type of signal is exactly the functional form on which the method is most effective. As described in Sec. 4.1, FDFA operates by eliminating the frequencies with largest amplitudes, so its maximum efficiency is reached when trends consists of few isolated frequencies with high power. In time series where trends are spread over a large portion of the spectrum or are too entwined with the noise frequencies, FDFA fails since it irremediably corrupts

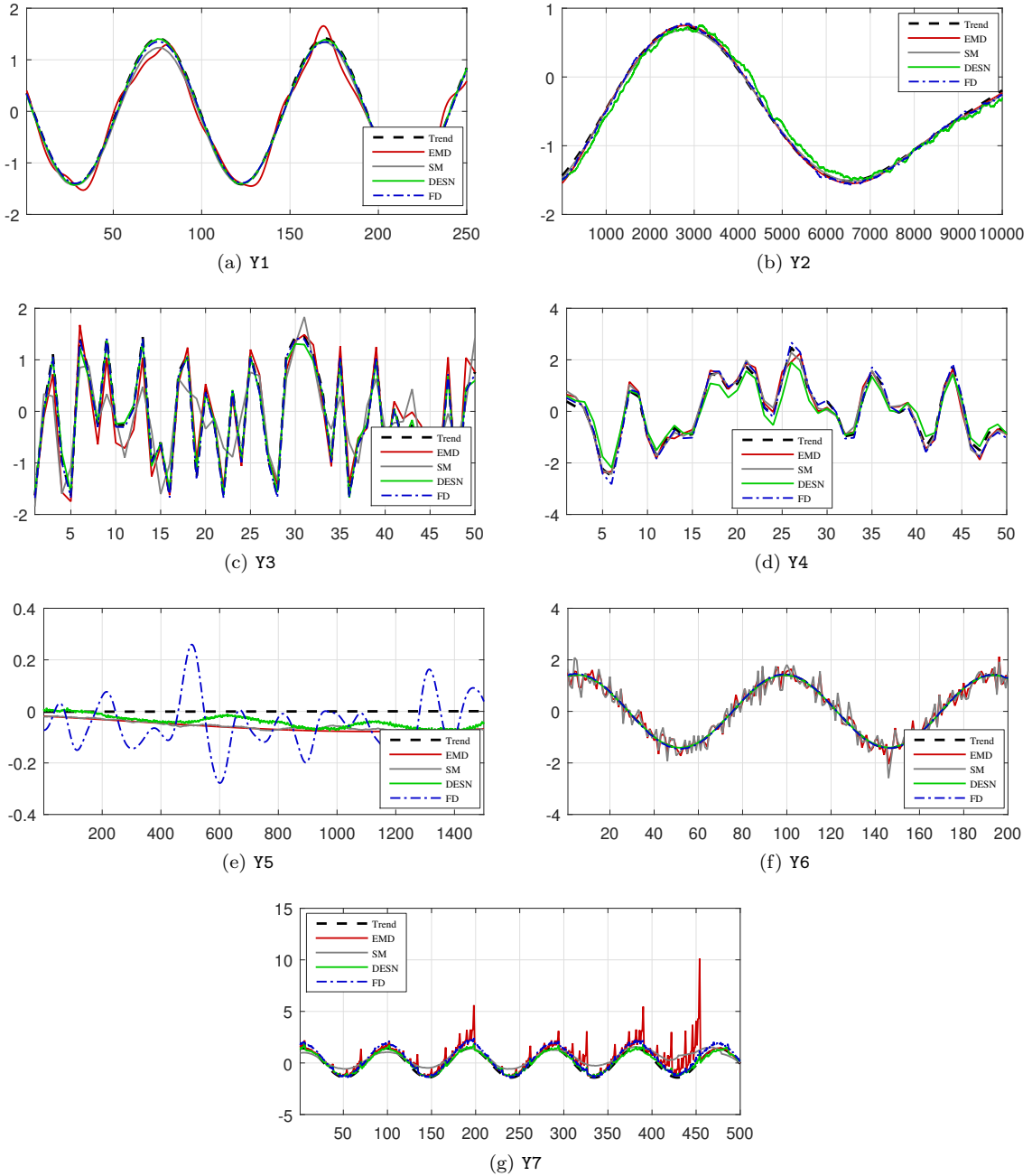


Figure 1: Trends identified on the different signals. The function depicted with black dashed lines represents the trend of the original time series. The colored lines represent the trends identified using DESN, EMD, FDFA, and SM.

the noise scaling properties. It is important to point out that, however, the original FDFA method as proposed in [9] works only as a low-pass filter without taking into account amplitudes, so its limitations are even more evident in these particular cases. SM and EMD, instead, do not perform well on this time series, i.e., Y1. While this is a common issue with EMD applied to sinusoidal signals, with SM we can observe in the example of Fig. 2 a crossover that breaks the global scaling. This crossover is given by the action of the smoothing algorithm only at certain scales determined by its span parameter.

Perhaps surprisingly, on the second time series, Y2, whose signal is a linear combination of low-frequency sinusoids with variable amplitudes and frequency, all methods perform equally well. This is probably due to the substantial separation in frequency between signal (the trend) and noise in the series.

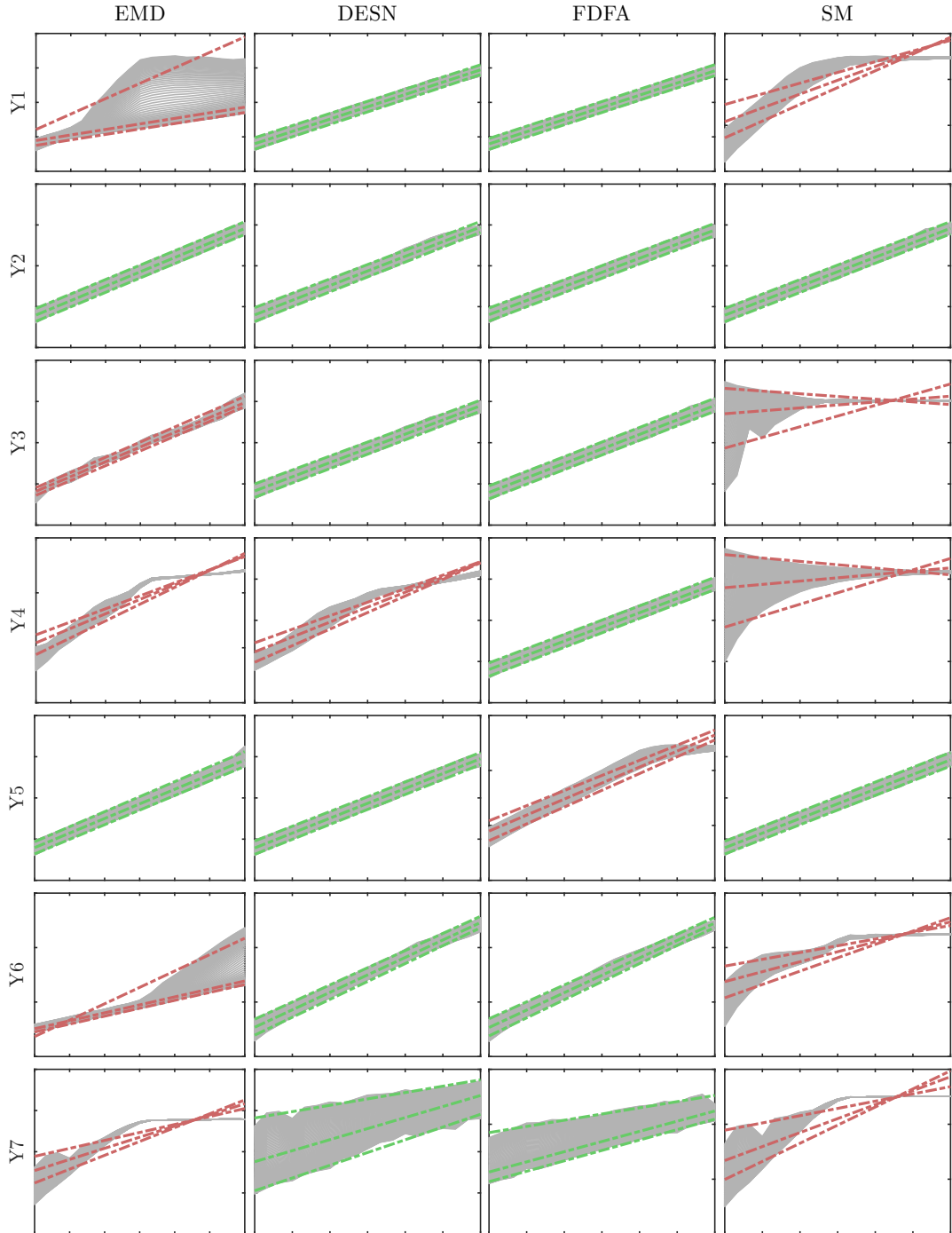


Figure 2: Fluctuation function scaling of the detrended time series. Only one instance of each test in Table 4 is reported here. The least-square fittings are highlighted in green when they correspond to a good-quality scaling function; in red otherwise.

On the third series Y_3 , we obtain similar results with the ones of the first test. This is somewhat expected, since the signal is conceptually similar to Y_1 , being composed by a periodic series made of the first 100 digits of π .

The series Y_4 is a more complex version of Y_2 , since the signal is composed by a linear combination of sinusoids, but in this case the frequencies are allowed to reach much higher values. In this case, only FDFA succeeds in detrending the series correctly. As explained above, the procedure, as it was

implemented here, does not filter trends according to their frequency values, but instead according to their amplitude, so it is effective independently of their position in the spectrum. EMD and SM, on the other hand, are designed with the underlying assumption of “slow” trends, so such methods are not able to correctly filter rapidly-varying trends. DESN, on the other hand, does not perform any explicit assumption regarding the trend. However, we note that the prediction of a high-frequency signal is inherently more challenging. In fact, as shown by the results the scaling of the fluctuation function is not consistent with a power-law in the DESN case.

Time series Y5 is a classic example where the FDFA method fails. In this case, the signal does not consist of isolated frequencies, so the filtering alters the signal by creating a crossover at larger scales. Other methods, instead, perform well on this time series, given its regular behavior in the time domain.

The time series Y6 is composed by the same trend of Y1 but its noise is antipersistent. Analogously to what we have observed for Y1, only DESN and FDFA succeed in removing the trend on such a time series.

In every test, the estimation of $\mathbf{n1}$ and $\mathbf{n2}$ resulted to be monofractal, as confirmed by the estimated MFWs shown in Table 4. The only exception is in the outcome given by EMD on Y5, where we detect on $\hat{n}(t)$ the presence of a fair (but spurious) multiscaling, which is not present in the ground-truth signal $\mathbf{n1}$.

Time series Y7 is the only series possessing a multifractal scaling. As we can observe from the results, only DESN and FDFA produce a correct scaling outcomes, even if the results are slightly corrupted, as expected by the higher complexity of such a time series. The calculated Hurst coefficient is slightly overestimated by DESN while it is underestimated by FDFA. The principal difference in performance between such two approaches lies in the estimated multifractal spectrum width. In fact, in this case the estimate obtained with DESN is significantly closer to the ground truth, while FDFA considerably underestimates its value, suggesting a process with far less multifractal properties. Moreover, we can observe that both methods overestimate the asymmetry with a bias on the left side of the spectrum. In the case of DESN, this can be explained by considering that the right part of the spectrum corresponds to the smaller fluctuations, which are more easily altered by the ESN prediction error.

4.3 Sunspot data

Here we consider the daily sunspot number time series [1]. The dataset contains more than 70000 records and it is characterized by a trend given by the well-known 11-year cycle of the sun. Such a dataset has been already used by other authors in the (multi)fractal time series analysis context – e.g, see [13, 20] and references therein.

For this test, we configured FDFA with $\tau_{\text{freq}} = 150$ and $\tau_{\text{time}} = 500$. In the EMD case, we set the weight parameter $\eta_{\text{EMD}} = 0.5$ in the cost function. For SM, we set the span $\sigma = 1000$, the weight parameter $\eta_{\text{SM}} = 0.1$, and we used the algorithm 2. For DESN, we set the reservoir size $N_r = 500$, the regularization coefficient $\lambda = 0.05$, and the spectral radius $\rho = 0.99$. For DESN, we compared two settings with different numbers k of forecast models, namely $k = 10$ and $k = 30$, which produced slightly different, yet qualitatively comparable results. Since there is no known ground truth for the sunspot time series, in this section we compare our results with the properties reported in other works [13, 20].

In Table 5, we show the values of the Hurst coefficient and the width of the multifractal spectrum. As we can see in the table, all four methods, when suitably tuned, agree on the persistence of the process up to fluctuations of ~ 0.05 in the Hurst coefficient values. Such values are also similar to the coefficient $H = 0.73$ reported in Ref. [20], where an adaptive detrending is performed on the time series – please notice that the authors of [20] use the monthly sunspot time series. Surprisingly, the Hurst coefficient retrieved with DESN using $k = 10$ is closer with respect to the other methods, while the outcome obtained with $k = 30$ is slightly higher. By assuming that the true value lies in-between the general consensus, this may suggest that a suitable dimension of the ESN ensemble has to be chosen in order to obtain best performance, even if the observed variability is in general fairly low. By looking at the MFW, we observe that DESN is not in agreement with the other detrending methods and, to a lower extent, also on the asymmetry Θ . In fact, even if all methods agree on the right-sided multifractal nature of the series, both DESN configurations denote a lower degree of multifractality and lower asymmetry. However, it is worth noting that the MFW value estimated by DESN is much closer to the values reported in Ref. [13], while the degree of asymmetry is still different. It is worth pointing out that, the authors of [13] did not perform any detrending in their work. This was possible by exploiting the fact that the underlying trend

Table 4: Average values and standard deviations (where applicable) of Hurst and width of the multifractal spectrum (MFW) of the noise estimated on each time series along with the ground truth (GT) evaluated on the noise. The asymmetry Θ of the multifractal spectrum (8) of the series Y7 is reported in brackets. The standard deviation is not defined in the results of FDFA on series Y7, since the values are deterministic. The cases in which the detrending method did not succeed in preserving the noise self-similarity are denoted with “n.s.”.

	ID	GT	DESN	FDFA	SM	EMD
Hurst	Y1	0.695	0.718 ± 0.007	0.705 ± 0.007	n.s.	n.s.
	Y2	0.695	0.719 ± 0.007	0.690 ± 0.004	0.703 ± 0.007	0.701 ± 0.006
	Y3	0.695	0.690 ± 0.006	0.702 ± 0.006	n.s.	n.s.
	Y4	0.695	n.s.	0.687 ± 0.002	n.s.	n.s.
	Y5	0.695	0.727 ± 0.006	n.s.	0.711 ± 0.006	0.711 ± 0.007
	Y6	0.303	0.318 ± 0.003	0.314 ± 0.002	n.s.	n.s.
	Y7	0.883	1.021 ± 0.003	0.793	n.s.	n.s.
MFW (Θ)	Y1	0.022	0.027 ± 0.012	0.026 ± 0.006	n.s.	n.s.
	Y2	0.022	0.032 ± 0.014	0.034 ± 0.013	0.028 ± 0.011	0.023 ± 0.009
	Y3	0.022	0.029 ± 0.008	0.024 ± 0.006	n.s.	n.s.
	Y4	0.022	n.s.	0.037 ± 0.010	n.s.	n.s.
	Y5	0.022	0.019 ± 0.007	n.s.	0.018 ± 0.005	0.102 ± 0.041
	Y6	0.032	0.040 ± 0.008	0.043 ± 0.002	n.s.	n.s.
	Y7	1.192 (0.048)	1.116 ± 0.046 (0.397 ± 0.060)	0.593 (0.849)	n.s.	n.s.

is very slow and a number of sufficient data points can be analyzed by considering scales lower than half of the dominating periodicity. In Fig. 3, we show the trends identified using the different approaches. As it is possible to observe, the trend calculated by DESN correctly recognizes the characteristic 11-year cycle of the sunspot time series. In Fig. 4, we show the results of the scaling of the fluctuation function obtained by using the two configurations of DESN.

The general agreement of the values estimated by DESN with other methods offers a sound justification for the quality and reliability of the proposed detrending method.

Table 5: Hurst exponent, MFW, and asymmetry (Θ) of the detrended sunspot time series, estimated using different detrending methods.

Method	Hurst	MFW	Θ
DESN ($k = 10$)	0.772 ± 0.0003	0.616 ± 0.0560	-0.393 ± 0.0536
DESN ($k = 30$)	0.820 ± 0.0002	0.694 ± 0.0614	-0.492 ± 0.0412
FDFA	0.688	1.205	-0.556
SM	0.680	1.118	-0.726
EMD	0.713	1.111	-0.742

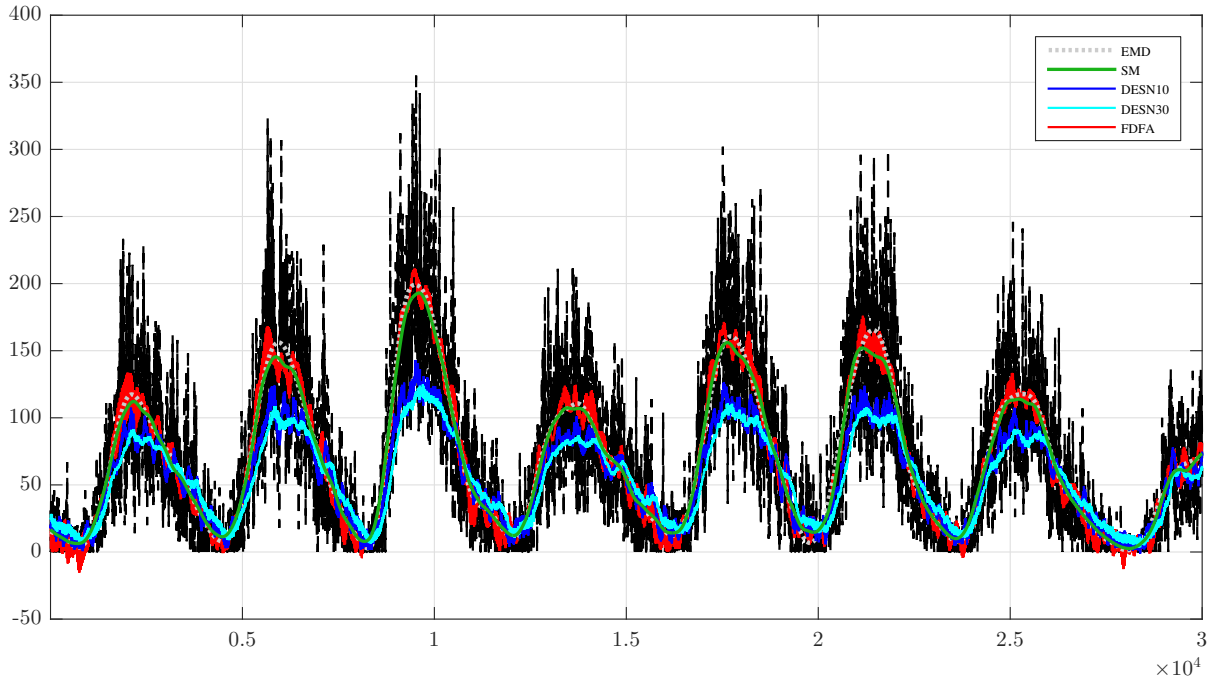


Figure 3: Trends identified on the sunspot time series. The function depicted with black dashed lines represent the original time series. The colored lines represent the trends identified using EMD, FDFA, SM, and DESN with $k = 10$ and $k = 30$.

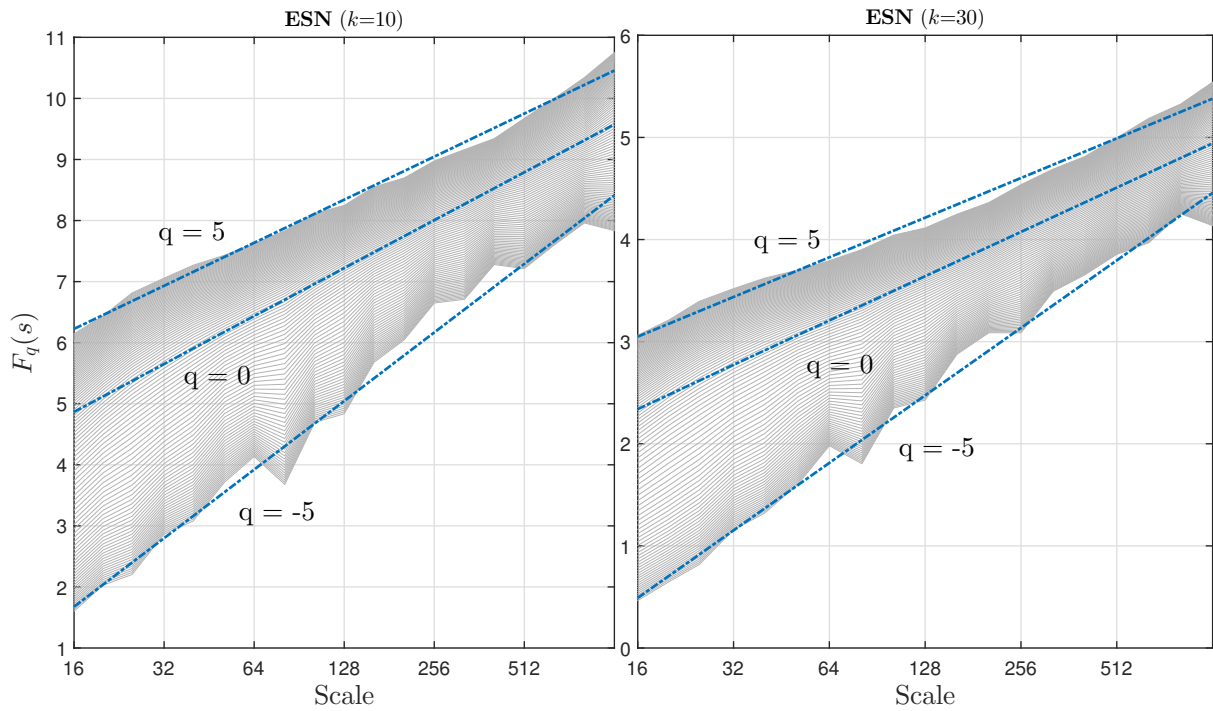


Figure 4: Scaling properties of the (detrended) sunspot time series obtained with DESN for two settings of the ensemble parameter k .

5 Conclusions

In this paper, we have explored the possibility of identifying and removing trends in a given time series by means of an echo state network, a particular type of recurrent neural network. The proposed method, called DESN, allowed us to filter out trends without the need to model time series *a priori* nor by performing a windowed fitting as proposed in other detrending approaches. This fact is a byproduct of the capability of recurrent neural networks to learn and predict complex dynamical processes under loose assumptions. Our main assumption here was a different degree of predictability involving the noise and trend components. We exploited such an assumption as a separating criterion. Notably, we have used an ensemble of echo state networks as a filter, operating with a standard configuration and trained using the linear regression as a readout mechanism. Many other approaches exist both for designing the reservoir and for training the readout [14, 39], which could be evaluated depending on specific problem at hand.

As a first benchmarking task, we have analyzed the performance of DESN and other detrending techniques taken from the literature on several synthetic time series. Such time series were generated using different types of trends. The quality of the detrending was evaluated by comparing the properties of the estimated noise with respect to the well-known ground truths. Calculations of self-similarity (Hurst) exponent and properties of the multifractal spectrum was performed in all cases by means of the multifractal detrended fluctuation analysis procedure, a consolidated method in this context. In most cases, the resulting fractal coefficients computed by DESN procedure agreed with the expected values and the noise self-similarity property was preserved by the detrending operation. However, in several occasions the other detrending methods were not able to perform a correct detrending, which resulted in an incorrect scaling of the fluctuation function. The proposed method, DESN, failed only in one instance, where the considered trend was composed by many sinusoids of significant power spread over the entire power spectrum.

As a second benchmarking test, we have studied the well-known sunspot time series, which is a well-known multifractal time series that has been analyzed in several related works [13, 20]. Our results suggested that the multifractal properties retrieved by using DESN were both qualitatively and quantitatively coherent with what suggested in other works taken from the literature. This fact strengthens the validity of the proposed data-driven detrending method based on echo state networks.

Appendix A Multifractal detrended fluctuation analysis

The MF DFA procedure is described thoroughly in [25] and it is reported briefly in the following. The procedure consists of five steps, three of which are identical to the DFA version. Let $x(t)$ be a time series of length N with compact support,

- *Step 1* : Evaluate $Y(i)$ as the cumulative sum (profile) of the series x_k :

$$Y(i) \equiv \sum_{k=1}^i [x_k - \langle x \rangle], \quad i = 1, \dots, N. \quad (10)$$

- *Step 2* : Separate $Y(i)$ in $N_s \equiv \text{int}(N/s)$ non-overlapping segments of equal length s . To account for non-zero remainders of the division, this operation is repeated in reverse order starting from the opposite end of the series, thus obtaining a total of $2N_s$ segments.
- *Step 3* : Perform local detrending by fitting a polynomial functional form on each of the $2N_s$ segments. Then determine the variance,

$$F^2(\nu, s) \equiv \frac{1}{s} \sum_{i=1}^s \left\{ Y[(\nu - 1)s + i] - y_\nu(i) \right\}^2, \quad (11)$$

for each segment $\nu = 1, \dots, N_s$ and

$$F^2(\nu, s) \equiv \sum_{i=1}^s \left\{ Y[N - (\nu - N_s)s + i] - y_\nu(i) \right\}^2 \quad (12)$$

for $\nu = N_s + 1, \dots, 2N_s$, where $y_\nu(i)$ is the fitted polynomial in segment ν . The order m of the fitting polynomial, $y_\nu(i)$, determines the extent of the (MF-)DFA in filtering out trends in the series, thus it has to be tuned according to the expected maximum trending order of the time series.

- *Step 4* : Compute the q th-order average of the variance over all segments,

$$F_q(s) \equiv \left\{ \frac{1}{2N_s} \sum_{\nu=1}^{2N_s} [F^2(\nu, s)]^{q/2} \right\}^{1/q}, \quad (13)$$

with $q \in \mathbb{R}$. The q -dependence of the fluctuations function $F_q(s)$ highlights the contribute of fluctuations at different orders of magnitude. For $q > 0$ ($q < 0$) only larger (smaller) fluctuations contribute mostly to the average in Eq. 13. For $q = 2$ the standard DFA procedure is obtained. The case $q = 0$ is not well defined with the averaging form in Eq. 13 and so a logarithmic form has to be employed,

$$F_0(s) = \exp \left\{ \frac{1}{2N_s} \sum_{\nu=1}^{2N_s} \ln [F^2(\nu, s)] \right\}. \quad (14)$$

Steps 2 to 4 are repeated for different time scales s , where all values of s have to be chosen such that $s \geq m + 2$ to allow for a meaningful fitting of data. It is also convenient to avoid scales $s > N/4$ because of the statistical unreliability of such small numbers N_s of segments considered.

- *Step 5* : Determine the scaling behavior of the fluctuation functions by analyzing log-log plots of $F_q(s)$ versus s for each value of q . If the series x_i is long-range power-law correlated, $F_q(s)$ is approximated (for large values of s) by the form

$$F_q(s) \sim s^{h(q)}. \quad (15)$$

The exponent $h(q)$ is the *generalized Hurst exponent*; for $q = 2$ and stationary time series, $h(q)$ reduces to the standard Hurst exponent, H . When the time series manifests a uniform scaling over all magnitudes of fluctuations - i.e. $h(q)$ is independent of q - the series is said monofractal. On the contrary, when $h(q)$ is spread over several values the series is multifractal.

Starting from Eq. 13 and using Eq. 15, it is straightforward to obtain

$$\sum_{\nu=1}^{N/s} [F(\nu, s)]^q \sim s^{qh(q)-1}, \quad (16)$$

where, for simplicity, it has been assumed that the length N of the series is a multiple of the scale s , such that $N_s = N/s$. The exponent

$$\tau(q) = qh(q) - 1 \quad (17)$$

corresponds to the multifractal generalization of the *mass exponent*. In case of positive stationary and normalized time series, $\tau(q)$ corresponds to the scaling exponent of the q -order partition function $Z_q(s)$. Another quantity that characterizes the multifractality of a series is the *singularity spectrum*, $D(\alpha)$, which is obtained by applying the Legendre transform to $\tau(q)$,

$$D(\alpha) = q\alpha - \tau(q), \quad (18)$$

where α is equal to the derivative $\tau'(q)$ and corresponds to the *Hölder* or *singularity exponent*. Using Eq. 17 it is possible to directly relate α and $D(\alpha)$ to $h(q)$, obtaining:

$$\alpha = h(q) + qh'(q) \quad \text{and} \quad D(\alpha) = q[\alpha - h(q)] + 1. \quad (19)$$

The singularity spectrum in Eq. 18 - also called *multifractal spectrum* (MFS) - allows to infer important information regarding the “degree of multifractality” and the specific sensitivity of the time series to fluctuations of different magnitudes. In fact, the width of the support of $D(\cdot)$ is an important quantitative indicator of the multifractal character of the series (the larger, the more fractal a series is). Also the codomain of $D(\cdot)$ encodes useful information, since it corresponds to the dimension of the subset of the times series domain which is characterized by the singularity exponent α .

Appendix B Echo state network

A schematic depiction of an ESN is shown in Fig. 5. The network can be divided in three components, namely the input layer, a recurrent reservoir, and a readout.

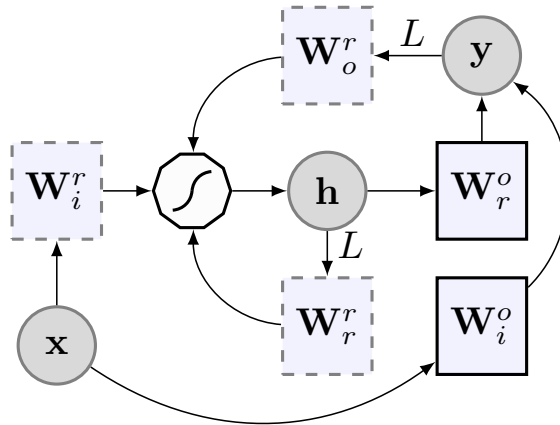


Figure 5: Schematic depiction of an ESN. The circles represent the input variables \mathbf{x} , the state variables \mathbf{h} and the output variables \mathbf{y} . The squares depicted with solid lines, \mathbf{W}_r^o and \mathbf{W}_i^o , are the trainable weight matrices of the readout, while the squares with dashed lines, \mathbf{W}_r^r , \mathbf{W}_o^r and \mathbf{W}_i^r , are random initialized weight matrices. The polygon represents the non-linear transformation of the neurons in the network and L represents the forward time-shift operator, which delays the values for a time step.

The current output of an ESN is computed in two distinct phases. First, the N_i -dimensional input vector $\mathbf{x}[n] \in \mathbb{R}^{N_i}$ is given as input to the recurrent reservoir, whose internal state $\mathbf{h}[n-1] \in \mathbb{R}^{N_r}$ is updated according to the state equation:

$$\mathbf{h}[n] = f_{\text{res}}(\mathbf{W}_i^r \mathbf{x}[n] + \mathbf{W}_r^r \mathbf{h}[n-1] + \mathbf{W}_o^r y[n-1]), \quad (20)$$

where $\mathbf{W}_i^r \in \mathbb{R}^{N_r \times N_i}$, $\mathbf{W}_r^r \in \mathbb{R}^{N_r \times N_r}$ and $\mathbf{w}_o^r \in \mathbb{R}^{N_r}$ are randomly initialized at the beginning of the learning process, and they remain unaltered afterwards. $f_{\text{res}}(\cdot)$ in Eq. (20) is a suitable non-linear function, typically a sigmoid, and $y[n-1] \in \mathbb{R}$ is the previous scalar output of the network. In our case, we have $f_{\text{res}}(\cdot) = \tanh(\cdot)$. In the second phase, the ESN prediction is computed according to:

$$y[n] = (\mathbf{W}_i^o)^T \mathbf{x}[n] + (\mathbf{W}_r^o)^T \mathbf{h}[n], \quad (21)$$

where $\mathbf{W}_i^o \in \mathbb{R}^{N_i}$, $\mathbf{W}_r^o \in \mathbb{R}^{N_r}$ are trainable connections. The difference between fixed and adaptable weight matrices is shown in Fig. 5 with the use of continuous and dashed lines, respectively.

Finally, a few words should be spent on the choice of the matrix \mathbf{W}_r^r . According to the ESN theory, the reservoir must satisfy the so-called ‘‘echo state property’’ (ESP) [31]. This means that the effect of a given input on the state of the reservoir must vanish in a finite number of time-instants. In this paper we adopt the widely used rule-of-thumb that suggests to rescale the matrix \mathbf{W}_r^r to have $\rho(\mathbf{W}_r^r) < 1$, where $\rho(\cdot)$ denotes the spectral radius.

To determine the weight matrices in the readout, let us consider a sequence of Q desired input-outputs pairs given by:

$$(\mathbf{x}[1], d[1]) \dots, (\mathbf{x}[Q], d[Q]), \quad (22)$$

while the output is given by:

$$d[t] = x[t + m], \quad (23)$$

where m define the forecast horizon. In the initial phase of training, called ‘state harvesting’, the inputs are fed to the reservoir in accordance with Eq. (20), producing a sequence of internal states $\mathbf{h}[1], \dots, \mathbf{h}[Q]$. Since, by definition, the outputs of the ESN are not available for feedback, the desired output is used

instead in Eq. (21) (so-called “teacher forcing”). The states are stacked in a matrix $\mathbf{H} \in \mathbb{R}^{Q \times N_i + N_r}$ and the desired outputs in a vector $\mathbf{d} \in \mathbb{R}^Q$:

$$\mathbf{H} = \begin{bmatrix} \mathbf{x}^T[1], \mathbf{h}^T[1] \\ \vdots \\ \mathbf{x}^T[Q], \mathbf{h}^T[Q] \end{bmatrix}, \quad (24)$$

$$\mathbf{d} = \begin{bmatrix} d[1] \\ \vdots \\ d[Q] \end{bmatrix}. \quad (25)$$

The initial D rows from Eq. (24) and Eq. (25) should be discarded, since they refer to a transient phase in the ESN’s behavior. We refer to them as the washout elements.

At this point the resulting training problem is a standard linear regression, which can be solved in a large variety of ways. We used the least-square regression (LSR), which is the algorithm originally proposed for training the readout [23]. It consists in the following regularized least-square problem:

$$\mathbf{w}_{\text{ls}}^* = \arg \min_{\mathbf{w} \in \mathbb{R}^{N_i + N_r}} \frac{1}{2} \|\mathbf{H}\mathbf{w} - \mathbf{d}\|_2^2 + \frac{\alpha}{2} \|\mathbf{w}\|_2^2, \quad (26)$$

where $\mathbf{w} = [\mathbf{w}_i^o \ \mathbf{w}_r^o]^T$ and $\alpha \in \mathbb{R}^+$ is a positive scalar known as *regularization factor*. A solution of problem (26) can be obtained in closed form as:

$$\mathbf{w}_{\text{ls}}^* = (\mathbf{H}^T \mathbf{H} + \alpha \mathbf{I})^{-1} \mathbf{H}^T \mathbf{d}. \quad (27)$$

Whenever $N_r + N_i > Q$, Eq. (27) can be computed more efficiently by rewriting it as:

$$\mathbf{w}_{\text{ls}}^* = \mathbf{H}^T (\mathbf{H}\mathbf{H}^T + \alpha \mathbf{I})^{-1} \mathbf{d}. \quad (28)$$

References

- [1] Daily sunspot number. URL <http://www.sidc.be/silso/datafiles>. last accessed on 01-Jul-2015.
- [2] J. Barunik and L. Kristoufek. On Hurst exponent estimation under heavy-tailed distributions. *Physica A: Statistical Mechanics and its Applications*, 389(18):3844–3855, 2010. doi: 10.1016/j.physa.2010.05.025.
- [3] A. Bashan, R. Bartsch, J. W. Kantelhardt, and S. Havlin. Comparison of detrending methods for fluctuation analysis. *Physica A: Statistical Mechanics and its Applications*, 387(21):5080–5090, 2008. doi: 10.1016/j.physa.2008.04.023.
- [4] W. Bialek, I. Nemenman, and N. Tishby. Predictability, complexity, and learning. *Neural Computation*, 13(11):2409–2463, 2001. doi: 10.1162/089976601753195969.
- [5] F. Bianchi, E. De Santis, A. Rizzi, and A. Sadeghian. Short-term electric load forecasting using echo state networks and PCA decomposition. *Access, IEEE*, PP(99):1–1, 2015. ISSN 2169-3536. doi: 10.1109/ACCESS.2015.2485943.
- [6] F. M. Bianchi, S. Scardapane, A. Uncini, A. Rizzi, and A. Sadeghian. Prediction of telephone calls load using echo state network with exogenous variables. *Neural Networks*, 71:204–2013, 2015. doi: 10.1016/j.neunet.2015.08.010.
- [7] Z. Chen, P. Ch., Ivanov, K. Hu, and H. E. Stanley. Effect of nonstationarities on detrended fluctuation analysis. *Physical Review E*, 65:041107, Apr. 2002. doi: 10.1103/PhysRevE.65.041107.
- [8] A. Chhabra and R. V. Jensen. Direct determination of the $f(\alpha)$ singularity spectrum. *Physical Review Letters*, 62:1327–1330, Mar 1989. doi: 10.1103/PhysRevLett.62.1327.
- [9] C. V. Chianca, A. Ticona, and T. J. P. Penna. Fourier-detrended fluctuation analysis. *Physica A: Statistical Mechanics and its Applications*, 357(3):447–454, 2005. doi: 10.1016/j.physa.2005.03.047.
- [10] J. P. Crutchfield and D. P. Feldman. Regularities unseen, randomness observed: Levels of entropy convergence. *Chaos: An Interdisciplinary Journal of Nonlinear Science*, 13(1):25–54, 2003. doi: 10.1063/1.1530990.
- [11] J. Dambre, D. Verstraeten, B. Schrauwen, and S. Massar. Information processing capacity of dynamical systems. *Scientific Reports*, 2, 2012. doi: 10.1038/srep00514.
- [12] J. G. De Gooijer and R. J. Hyndman. 25 years of time series forecasting. *International Journal of Forecasting*, 22(3):443–473, 2006. doi: 10.1016/j.ijforecast.2006.01.001.
- [13] S. Drożdż and P. Oświęcimka. Detecting and interpreting distortions in hierarchical organization of complex time series. *Physical Review E*, 91(3):030902, 2015. doi: 10.1103/PhysRevE.91.030902.
- [14] X. Dutoit, B. Schrauwen, J. Van Campenhout, D. Stroobandt, H. Van Brussel, and M. Nuttin. Pruning and regularization in reservoir computing. *Neurocomputing*, 72(7):1534–1546, 2009.
- [15] M. Fernández-Martínez, M. Sánchez-Granero, and J. T. Segovia. Measuring the self-similarity exponent in lévy stable processes of financial time series. *Physica A: Statistical Mechanics and its Applications*, 392(21):5330–5345, 2013. doi: 10.1016/j.physa.2013.06.026.

- [16] P. Flandrin, G. Rilling, and P. Goncalves. Empirical mode decomposition as a filter bank. *IEEE Signal Processing Letters*, 11(2):112–114, Feb. 2004. doi: 10.1109/LSP.2003.821662.
- [17] J. Gao, Y. Cao, W.-W. Tung, and J. Hu. *Multiscale Analysis of Complex Time Series: Integration of Chaos and Random Fractal Theory, and Beyond*. John Wiley & Sons, New York, NY, USA, 2007.
- [18] D. Grech and G. Pamula. On the multifractal effects generated by monofractal signals. *Physica A: Statistical Mechanics and its Applications*, 392(23):5845–5864, 2013. doi: 10.1016/j.physa.2013.07.045.
- [19] L. K. Hansen and P. Salamon. Neural network ensembles. *IEEE Transactions on Pattern Analysis & Machine Intelligence*, 12(10):993–1001, Oct. 1990. doi: 10.1109/34.58871.
- [20] J. Hu, J. Gao, and X. Wang. Multifractal analysis of sunspot time series: the effects of the 11-year cycle and Fourier truncation. *Journal of Statistical Mechanics: Theory and Experiment*, 2009(02):P02066, 2009. doi: 10.1088/1742-5468/2009/02/P02066.
- [21] K. Hu, P. Ch., Ivanov, Z. Chen, P. Carpena, and H. E. Stanley. Effect of trends on detrended fluctuation analysis. *Physical Review E*, 64:011114, Jun. 2001. doi: 10.1103/PhysRevE.64.011114.
- [22] N. E. Huang, M-L C. Wu, S. R. Long, S S.P. Shen, W. Qu, P. Gloersen, and K. L. Fan. A confidence limit for the empirical mode decomposition and Hilbert spectral analysis. *Proceedings of the Royal Society of London A: Mathematical, Physical and Engineering Sciences*, 459(2037):2317–2345, 2003. ISSN 1364-5021. doi: 10.1098/rspa.2003.1123.
- [23] H. Jaeger. The echo state approach to analysing and training recurrent neural networks. Technical report, Technical Report GMD Report 148, German National Research Center for Information Technology, 2001.
- [24] J. W. Kantelhardt. Fractal and multifractal time series. In R. A. Meyers, editor, *Mathematics of Complexity and Dynamical Systems*, pages 463–487. Springer, New York, 2011. ISBN 978-1-4614-1805-4. doi: 10.1007/978-1-4614-1806-1_30.
- [25] J. W. Kantelhardt, S. A. Zschiegner, E. Koscielny-Bunde, S. Havlin, A. Bunde, and H. E. Stanley. Multifractal detrended fluctuation analysis of nonstationary time series. *Physica A: Statistical Mechanics and its Applications*, 316(1):87–114, 2002. doi: 10.1016/S0378-4371(02)01383-3.
- [26] L. Livi, E. Maiorino, A. Rizzi, and A. Sadeghian. On the long-term correlations and multifractal properties of electric arc furnace time series. *International Journal of Bifurcation and Chaos*, 2015.
- [27] L. Livi, A. Sadeghian, and H. Sadeghian. Discrimination and characterization of Parkinsonian rest tremors by analyzing long-term correlations and multifractal signatures. *ArXiv preprint arXiv:1504.02756*, Apr. 2015.
- [28] J T-H. Lo. Synthetic approach to optimal filtering. *IEEE Transactions on Neural Networks*, 5(5):803–811, Sep. 1994. doi: 10.1109/72.317731.
- [29] J T-H. Lo and J. Nave. Adaptive neural filters with fixed weights. In *Proceedings of the IEEE International Joint Conference on Neural Networks*, pages 2147–2152, Orlando, FL, Aug. 2007. doi: 10.1109/IJCNN.2007.4371290.
- [30] J T-H. Lo and L. Yu. Recursive neural filters and dynamical range transformers. *Proceedings of the IEEE*, 92(3):514–535, Mar. 2004. ISSN 0018-9219. doi: 10.1109/JPROC.2003.823148.
- [31] M. Lukoševičius and H. Jaeger. Reservoir computing approaches to recurrent neural network training. *Computer Science Review*, 3(3):127–149, 2009. doi: 10.1016/j.cosrev.2009.03.005.
- [32] M. S. Movahed and E. Hermanis. Fractal analysis of river flow fluctuations. *Physica A: Statistical Mechanics and its Applications*, 387(4):915–932, 2008. doi: 10.1016/j.physa.2007.10.007.
- [33] R. Nagarajan. Reliable scaling exponent estimation of long-range correlated noise in the presence of random spikes. *Physica A: Statistical Mechanics and its Applications*, 366:1–17, 2006. doi: 10.1016/j.physa.2005.10.020.
- [34] P. Oświęcimka, J. Kwapien, and S. Drożdż. Wavelet versus detrended fluctuation analysis of multifractal structures. *Physical Review E*, 74:016103, Jul. 2006. doi: 10.1103/PhysRevE.74.016103.
- [35] A. G. Parlos, K. T. Chong, and A. F. Atiya. Application of the recurrent multilayer perceptron in modeling complex process dynamics. *IEEE Transactions on Neural Networks*, 5(2):255–266, Mar. 1994. doi: 10.1109/72.279189.
- [36] X-Y. Qian, G-F. Gu, and W-X. Zhou. Modified detrended fluctuation analysis based on empirical mode decomposition for the characterization of anti-persistent processes. *Physica A: Statistical Mechanics and its Applications*, 390(23):4388–4395, 2011. doi: 10.1016/j.physa.2011.07.008.
- [37] M. A. Riley, S. Bonnette, N. Kuznetsov, S. Wallot, and J. Gao. A tutorial introduction to adaptive fractal analysis. *Frontiers in Physiology*, 3, 2012. doi: 10.3389/fphys.2012.00371.
- [38] M. Sánchez, J. E. Trinidad, J. García, and M. Fernández. The effect of the underlying distribution in Hurst exponent estimation. *PLoS ONE*, 10(5):e0127824–e0127824, 2014. doi: 10.1371/journal.pone.0127824.
- [39] S. Scardapane, G. Nocco, D. Comminiello, M. Scarpiniti, and A. Uncini. An effective criterion for pruning reservoir’s connections in Echo State Networks. In *Proceedings of the IEEE International Joint Conference on Neural Networks*, pages 1205–1212, Beijing, China, Jul. 2014.
- [40] F. Serinaldi. Use and misuse of some Hurst parameter estimators applied to stationary and non-stationary financial time series. *Physica A: Statistical Mechanics and its Applications*, 389(14):2770–2781, 2010. doi: 10.1016/j.physa.2010.02.044.
- [41] Y.-H. Shao, G.-F. Gu, Z.-Q. Jiang, W.-X. Zhou, and D. Sornette. Comparing the performance of FA, DFA and DMA using different synthetic long-range correlated time series. *Scientific Reports*, 2, 2012. doi: 10.1038/srep00835.
- [42] A. Topchy, A. K. Jain, and W. Punch. Clustering ensembles: models of consensus and weak partitions. *IEEE Transactions on Pattern Analysis and Machine Intelligence*, 27(12):1866–1881, Oct. 2005. doi: 10.1109/TPAMI.2005.237.
- [43] H. Wendt and P. Abry. Multifractality tests using bootstrapped wavelet leaders. *IEEE Transactions on Signal Processing*, 55(10):4811–4820, Oct. 2007. doi: 10.1109/TSP.2007.896269.
- [44] Z. Wu, N. E. Huang, S. R. Long, and C.-K. Peng. On the trend, detrending, and variability of nonlinear and nonstationary time series. *Proceedings of the National Academy of Sciences*, 104(38):14889–14894, 2007. doi: 10.1073/pnas.0701020104.